Applied Catalysis B: Environmental 132–133 (2013) 363–369

Contents lists available at SciVerse ScienceDirect

Applied Catalysis B: Environmental

journal homepage: www.elsevier.com/locate/apcatb

Synthesis and catalysis of copper sulfide/carbon nanodots for oxygen reduction in direct methanol fuel cells

Zih-Yu Shih, Arun Prakash Periasamy, Pin-Che Hsu, Huan-Tsung Chang*

Department of Chemistry, National Taiwan University, 1, Section 4, Roosevelt Road, Taipei 106, Taiwan

ARTICLE INFO

Article history:
Received 16 September 2012
Received in revised form
13 November 2012
Accepted 3 December 2012
Available online 13 December 2012

Keywords:
Carbon nanodots
Cathode catalyst
$Cu_{2-x}S$
Fuel cells
Oxygen reduction reaction

ABSTRACT

We have fabricated $Cu_{2-x}S$/carbon nanodot (C dot) electrodes for direct methanol fuel cells (DMFCs). To the best of our knowledge, this is the first time that $Cu_{2-x}S$/C dot nanomaterials (NMs) were proposed to be used as a cathode catalyst for oxygen reduction reaction (ORR) in acidic media. The structural characterizations revealed that $Cu_{2-x}S$ alloy possessed two types of crystalline phases, such as Cu_9S_5 and Cu_2S in the structure of $Cu_{2-x}S$/C dot NMs. The onset potential of the ORR for $Cu_{2-x}S$/C dot NMs is 0.92 V (vs. Ag/AgCl), revealing a good ORR activity of these NMs. The $Cu_{2-x}S$/C dot electrodes (mass loading: 2.26 mg cm^{-2}) provide a mean limiting density of −1.77 mA cm^{-2} at a scan rate of 5 mV s^{-1} and rotation rate of 3600 rpm. Electrochemical impedance spectrometry (EIS) results revealed that the charge-transfer resistance (R_{ct}) of the $Cu_{2-x}S$/C dots was smaller than that of $Cu_{2-x}S$/CNT. In addition, compared with Pt/C electrodes, $Cu_{2-x}S$/C dot electrodes were more tolerant against MeOH poisoning. The low-cost, electrochemically stable, and highly active $Cu_{2-x}S$/C dot electrode has great potential for use in DMFCs.

1. Introduction

Efficient catalysts for the oxygen reduction reaction (ORR; $O_2 + 4H^+ + 4e^- \rightarrow 2H_2O$) are essential for the fabrication of high-performance direct methanol fuel cells (DMFCs) [1]. When using a Pt cathode, the ORR rate is much slower than that of its anodic counterpart, leading to significant overpotential that reduces the performance of DMFCs [2]. Many nanomaterials (NMs) such as nitrogen-doped carbon [3–6], CuS [7], and $CoSe_2$/C [8,9] have been prepared and employed as effective catalysts for high-rate ORR kinetics by taking advantage of their large surface area and high catalytic activities [10,11]. Low-cost MS (M = Co and Cu) exhibits metal-like electrical conductivity, a property that has attracted significant interest in electrochemistry; however, current MS electrodes have much lower ORR activities than Pt electrodes [12,13].

Carbon supports are commonly used in fuel cells to improve the electrochemical activity and stability of catalysts mainly because of their large surface area, low cost, and unique electrical properties [14–16]. Carbon-supported Co_3S_4 and $CoSe_2$ NMs with onset potential values of 0.67 V and 0.72 V, respectively, are more active in the ORR than a reversible hydrogen electrode in acidic media [12,16]. To strengthen the interaction between MS NMs and carbon supports, the direct growth of $Co_{1-x}S$ NMs on reduced graphene oxide has been demonstrated [12,13]. The reduced graphene oxide not only assists in the growth of small-sized $Co_{1-x}S$ NMs, which yields larger surface area, and thus higher electroactivity, but also enhances the ORR catalytic activity of the $Co_{1-x}S$ NMs through strong electrochemical coupling.

In this study, our goal is to fabricate high-performance cathodic catalysts in DMFCs using $Cu_{2-x}S$ NPs and carbon nanodots (C dots). Cuprous sulfide (Cu_2S) has been used extensively as a photonic material as it exerts two distinct localized surface plasmon resonance modes [17], as a cathode reaction catalyst in a vanadium redox flow battery [18], and as a catalyst for the nucleation of In_2S_3 nano-crystals [19]. Adsorbed onto the surface of a polymer such as polypropylene, Cu_2S is capable of catalyzing the molecular recognition of ammonia gas [20]. C dots have large surface area, good electrical conductivity, and excellent mechanical strength [14–16], while inexpensive $Cu_{2-x}S$ NPs exhibit high ORR activity. $Cu_{2-x}S$/C dot NMs were synthesized from $Cu(NO_3)_2$, C dots, and Na_2S (S^{2-} source) using polyvinylpyrrolidone (PVP) as a stabilizer. PVP is commonly used to enhance the dispersion and adhesion of NMs on substrates such as CNTs [21]. We investigated the roles that various carbon supports played in controlling the direct growth of $Cu_{2-x}S$ on their surfaces, and thus their catalytic efficiency for ORR.

2. Materials and methods

2.1. Materials

Commercially available copper nitrate (≥99.8 wt%), carbon nanotubes (30–40 nm O.D. × 5–9 μm length, CNTs), Vulcan XC-72R

* Corresponding author. Tel.: +886 2 33661171; fax: +886 2 33661171.
E-mail address: changht@ntu.edu.tw (H.-T. Chang).

0926-3373/$ – see front matter © 2012 Elsevier B.V. All rights reserved.
http://dx.doi.org/10.1016/j.apcatb.2012.12.004

carbon black (particle size ~ 50 nm), graphite powder (particle size ~ 2 μm), methanol (≥99.8 wt%), ethanol (≥99.8 wt%), and PVP (M_w 10,000) were purchased from Sigma (St. Louis, MO, USA). Sodium sulfide (≥99.5 wt%) and diamine hydrate (≥95 wt%) were purchased from Seedchem (Melbourne, VIC, Australia). Platinum on activated carbon (Pt/C, 40 wt%) was purchased from Alfa Aesar (Ward Hill, MA, USA). Coffee grounds were collected from used Blue Mountains coffee (Taipei, Taiwan). Nafion 117 (5 wt%) and sulfuric acid (≥99.8 wt%) were purchased from Fluka (Buchs, Switzerland). Highly purified water (18.2 MΩ cm) from a Milli-Q ultrapure system (London, UK) was used throughout this study.

2.2. Synthesis of C dots by a hydrothermal method

C dots were prepared from used coffee grounds of blue mountain coffee beans through a hydrothermal route according to our previous study [16]. We note that C dots prepared from different brands of coffee grounds were slightly different with respects to fluorescence quantum efficiency, yield, and surface properties. Used coffee ground was dried in an oven at 110 °C. After calcination at 300 °C for 2 h, black carbonized powder (~5 mg) was cooled to 20 °C and dispersed in ethanol (5 mL). The solution was then centrifuged at 3000 rpm for 10 min to remove large particles. The supernatant containing C dots was filtered through a 0.22-μM membrane to further remove large particles. The concentration of as-synthesized C dots was about 63.8 μg/mL.

2.3. Synthesis of C dots (C_{dh}) by laser irradiation

C dots (C_{dh}) were prepared from graphite powder through the laser irradiation method [22]. Nd:YAG pulsed laser with a wavelength of 1064 nm and power density of 6.0×10^6 W cm^{-2} was used to irradiate 0.1 mg of graphite powder dispersed in 0.5 mL of diamine hydrate. Stirring was employed during the laser irradiation to expedite the movement of carbon particles. After being irradiated for 2 h, a homogeneous black suspension was obtained, which was centrifuged (3000 rpm, 10 min) to separate the black carbon precipitate and the colorful supernatant. The supernatant was then filtered through a 0.22-μM membrane to remove the larger particles. The concentration of as-synthesized C_{dh} was about 72.3 μg/mL.

2.4. Preparation of $Cu_{2-x}S$/C dot, $Cu_{2-x}S$/CNT, $Cu_{2-x}S/C_{dh}$, and $Cu_{2-x}S$/carbon black NMs

$Cu(NO_3)_2$ (0.2 mL 0.5 M), Na_2S (0.2 mL 0.5 M), C dots (0–0.02 mg), and PVP (0.04 g) were mixed together with ethanol (final volume 2.6 mL). Each of the mixtures reacted separately in a Teflon autoclave at 120 °C for 4 h. The color of the mixture turned dark-green, indicating the formation of $Cu_{2-x}S$/C dot NMs. We then applied a similar procedure to prepare $Cu_{2-x}S$/CNT, $Cu_{2-x}S/C_{dh}$, and $Cu_{2-x}S$/carbon black NMs using CNTs, C_{dh}, and carbon black (0–0.2 mg), respectively, instead of C dots. Each $Cu_{2-x}S$/C dot, $Cu_{2-x}S$/CNT, $Cu_{2-x}S/C_{dh}$, and $Cu_{2-x}S$/carbon black NMs solution was subjected to sonication for at least 30 min and then to two centrifugation (6000 rpm, 10 min)/wash (EtOH, 1.5 mL) cycles. Each of the $Cu_{2-x}S$/C dot, $Cu_{2-x}S$/CNT, $Cu_{2-x}S/C_{dh}$, and $Cu_{2-x}S$/carbon black NMs was then re-dispersed in EtOH (1.0 mL) prior to use.

2.5. Characterization

Transmission electron microscopy (TEM) and high-resolution TEM (HRTEM) images of as-prepared NMs were recorded using JEOL JSM-1230 (Hitachi, Tokyo, Japan) and FEI Tecnai-G2-F20 (GCE-Market, NJ, USA) systems operating at 200 kV, respectively. High angle annular dark-field scanning TEM (HAADF-STEM) images were recorded using Philips Tecnai F20 G2 FEI-TEM (Roanoke, VA, USA) equipped with an energy-dispersive X-ray spectrometer (EDS). The as-prepared NMs were carefully deposited onto 400-mesh C-coated Ni grids and the excess solvents were evaporated at ambient temperature (25 °C) and pressure. For X-ray diffraction (XRD) studies, a PANalytical X'Pert PRO diffractometer (Almelo, Netherlands) with Cu Kα radiation (λ = 0.15418 nm) was used. X-ray photoelectron spectroscopy (XPS) measurement was conducted using a VG ESCA210 electron spectroscope from VG Scientific (West Sussex, UK). The binding energy (BE) for Au was used as an internal reference to eliminate the charging effect. The samples for XPS measurements were prepared by depositing drops of the as-prepared NMs onto Si substrates and then evaporating the solvents at ambient temperature and pressure. An Elan 6000 inductively coupled plasma mass spectrometer (ICP-MS) from Perkin-Elmer (Wellesley, MA, USA) was employed to determine Cu contents in the as-prepared $Cu_{2-x}S$/C dot, $Cu_{2-x}S$/CNT, $Cu_{2-x}S/C_{dh}$, and $Cu_{2-x}S$/carbon black NMs. Prior to ICP-MS measurements, the as-prepared $Cu_{2-x}S$/C dot and $Cu_{2-x}S$/CNT NMs were dissolved in 2% HNO_3. Photoluminescence images were recorded using an Olympus IX71 (Tokyo, Japan) fluorescence microscope with a DP70 digital camera. The excitation wavelength was in a range of 340–365 nm.

2.6. Fabrication of electrodes and electrocatalytic analysis

Aliquots ($Cu_{2-x}S$ catalyst mass loading: 2.26 mg cm^{-2}) of the as-synthesized NMs solutions were placed separately onto the clean glassy carbon surface of each RDE (diameter: 5 mm). After being air-dried for 1 h at ambient temperature, Nafion solution (0.5%, 1 μL) was placed onto each of the electrodes. A commercial Pt/C solution was used to prepare control electrodes in a similar way. Three-electrode electrochemical cells were constructed using one of the modified RDE as the working electrode, a Pt wire as the auxiliary electrode, and an Ag/AgCl electrode as the reference. The electrocatalytic activities of the as-synthesized NMs in the three-electrode cells were measured using a CHI 760D electrochemical workstation (Austin, TX, USA). Cyclic voltammetry (CV) measurements of the $Cu_{2-x}S$/C dot RDEs in O_2-saturated and N_2-saturated 0.5 M H_2SO_4 were conducted over a potential range from 0 to 1.0 V at a scan rate of 5 mV s^{-1}. Linear sweep voltammetry (LSV) measurements of the as-prepared RDEs in O_2-saturated 0.5 M H_2SO_4 were conducted over a potential range from 0 to 1.0 V at a scan rate of 5 mV s^{-1} with different rotation speeds. The kinetics of ORR occurring at the RDEs was explored using Koutecky–Levich equations:

$$\frac{1}{J} = \frac{1}{J_L} + \frac{1}{J_K} \quad (1)$$

$$J_L = 0.62nFC_0D_0^{2/3}\nu^{-1/6}\omega^{1/2} \quad (2)$$

$$J_K = nFkC_0 \quad (3)$$

where J is the measured current density, J_K and J_L are the kinetic and diffusion limiting current densities, respectively, n is the overall number of electrons transferred, F is the Faraday constant, C_0 is the O_2-saturated 0.5 M H_2SO_4 (~1.1×10^{-6} mol cm^{-3}), D_0 is the diffusion coefficient of O_2 (~1.4×10^{-5} cm^2 s^{-1}), ν is the kinetic viscosity of the solution (0.01 cm^2 s^{-1}), k is the kinetic rate constant, and ω is the rotation rate (rpm) [23]. The slopes of their best linear fit lines in Fig. 4B were used to calculate the number of electrons transferred (n) according to the Koutecky–Levich equation.

$Cu_{2-x}S$/C dot NMs and commercial Pt/C catalyst were conducted in 0.5 M H_2SO_4/1.0 M MeOH over the same potential range. The data were used to obtain Tafel plots to investigate MeOH tolerance of the electrodes. All electrochemical data were recorded over 10 reproducible cycles. The electrochemical impedance spectrometer

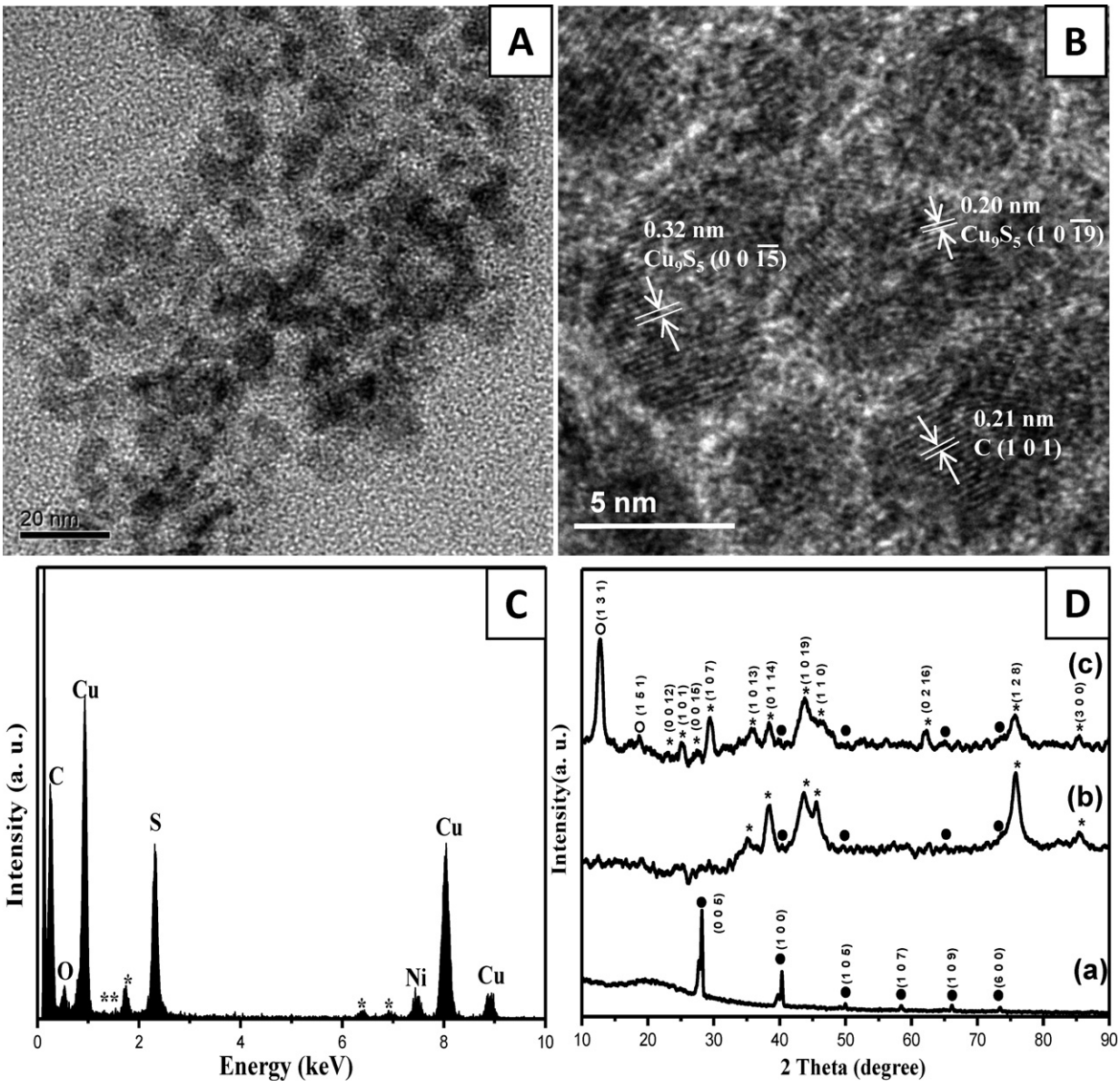

Fig. 1. (A) TEM, (B) high-resolution TEM images, and (C) EDS of $Cu_{2-x}S$/C dot NMs. Signals marked with asterisk belong to the elements present in the metallic cavity of the instrument. (D) Powder XRD patterns of (a) C dots, (b) $Cu_{2-x}S$/CNT, and (c) $Cu_{2-x}S$/C dot NMs. The solid circles indicate the diffraction peaks of the graphitic carbon, and the symbols (*) and (○) are assigned to the diffraction peaks of the digenite Cu_9S_5 and chalcocite Cu_2S, respectively.

(EIS) was employed at a 5-mV root-mean-square amplitude and scans over the range of 100 kHz to 1 Hz to determine the charge-transfer resistance between the electrode and the electrolyte.

3. Results and discussion

3.1. Characterization of $Cu_{2-x}S$/C dots

It is difficult to differentiate $Cu_{2-x}S$ NMs from C dots in the TEM image (Fig. 1A). Relatively, it is plausible to distinguish these NMs from their corresponding HRTEM image (Fig. 1B) [19]. The lattice spacings $d_{1\,0\,1}$ (0.21 nm) assigned to the C dots [24] and $d_{0\,0\,\overline{1\,5}}$ (0.32 nm) and $d_{1\,0\,\overline{1\,9}}$ (0.20 nm) assigned to the Cu_9S_5 NMs [25,26]. EDS pattern (Fig. 1C) confirms the existence of Cu, S, and C atoms in the $Cu_{2-x}S$/C dot NMs. We further confirmed the composition of the $Cu_{2-x}S$/C dot NMs. The diffraction peaks of C dots (curve a in Fig. 1D) are assigned to the sp^2 graphitic planes in reference to JCPDS card No. 26-1077 and 22-1069 [24,27]. The grain size of C dots calculated using Scherrer's formula [28] was approximately 12.9 nm. The diffraction peaks marked by an asterisk in curves b and c are readily indexed to digenite Cu_9S_5 (i.e., $Cu_{1.8}S$, JCPDS No. 26-0476) [29]. When compared with the standard pattern, the diffraction peaks were much broadened, revealing the formation of small crystallites [30]. The grain size of the $Cu_{2-x}S$ NMs was ca. 5.3 nm. The diffraction peaks marked by a symbol (○) in the curve c of Fig. 1D confirm the formation of chalcocite Cu_2S (JCPDS No. 12-0227) [31]. The plane (0 0 5) of C dots in $Cu_{2-x}S$/C dot NMs was not observed, because it was covered by the PVP. Thus, the as-synthesized $Cu_{2-x}S$/C dot NMs were comprised of both Cu_9S_5 and Cu_2S phases. When prepared at temperatures below and above 103.5 °C, Cu_2S exhibits monoclinic and hexagonal symmetries, respectively [32]. When performing the synthesis at 120 °C, we did obtain hexagonal $Cu_{2-x}S$ NMs in the presence of C dots.

We conducted high angle annular dark-field scanning TEM (HADDF-STEM) to identify the structures of $Cu_{2-x}S$/C dot NMs in Fig. S1A (see ESI). The bright sections are assigned to $Cu_{2-x}S$ NMs,

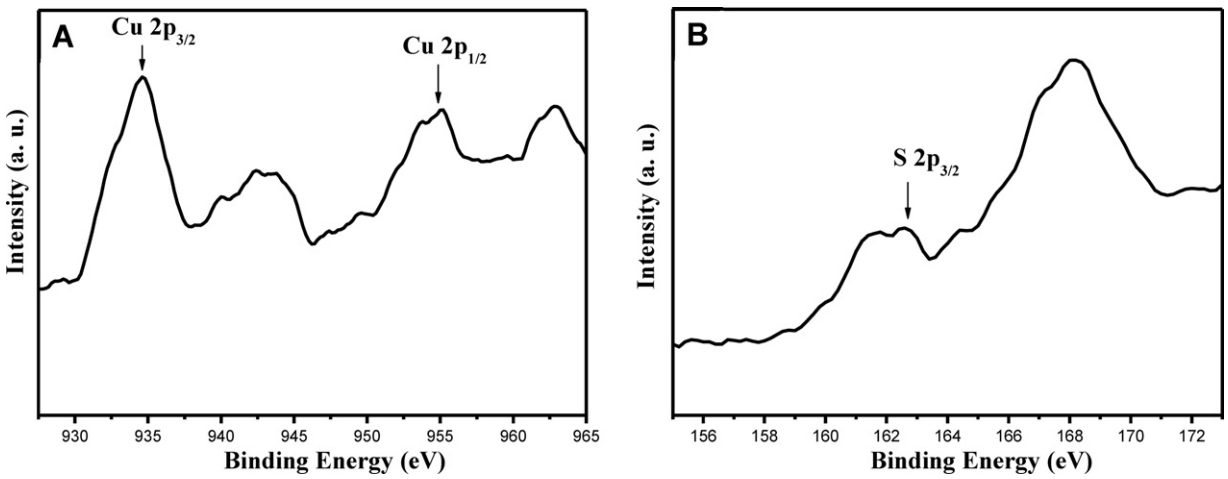

Fig. 2. XPS spectra of the (A) Cu 2p and (B) S 2p binding energy of the $Cu_{2-x}S$/C dot NMs.

while the gray regions are assigned to C dots. Corresponding EDS maps are provided in the insets to Fig. S1A, displaying that the Cu and S atoms were located in the same position. In other words, the $Cu_{2-x}S$ compounds are alloys. The electron diffraction pattern in Fig. S1B indicates that the $Cu_{2-x}S$/C dot NMs had a multicrystalline structure. To further confirm the position of the C dots, the fluorescence images in bright and dark fields are depicted in Fig. S1C and S1D, respectively. The dark-field fluorescence image displays aggregates of $Cu_{2-x}S$/C dot NMs, while the bright image revealed distribution of C dots on $Cu_{2-x}S$/C dot NMs, confirming the TEM and STEM results.

In XPS measurements, the $Cu_{2-x}S$/C dot NMs exhibited four distinguished BE peaks at 934.6, 943.3, 954.8, and 962.7 eV in Fig. 2A. The first two peaks are higher than 932.3 eV, which is assigned to $2p_{3/2}$ for Cu(0), while the last two are higher than 952.2 eV, which is assigned to $2p_{1/2}$ for Cu(0) [33]. Fig. 2B displays broad and overlapped BE peaks for $Cu_{2-x}S$/C dot NMs around 162.3 eV, showing the existence of S $2p_{3/2}$ in $Cu_{2-x}S$ [34]. The broad S $2p_{3/2}$ peaks of $Cu_{2-x}S$/C dot NMs were mainly due to the interaction of their electronic states with those of the C dots. There is no obvious shoulder in the higher energy region (>169 eV), implying that the surfaces of the $Cu_{2-x}S$/C dot NMs are stable [35]. Since $Cu_{2-x}S$ was bonded to the C dots in the $Cu_{2-x}S$/C dot NMs, the $Cu_{2-x}S$/C dot NMs and $Cu_{2-x}S$ may have different electrocatalytic activities [14–16].

3.2. Electrocatalytic activities of $Cu_{2-x}S$/C dots NMs electrodes

We tested the electrocatalytic activity of RDEs modified with $Cu_{2-x}S$/carbon black, $Cu_{2-x}S/C_{dh}$, $Cu_{2-x}S$/C dot, and $Cu_{2-x}S$/CNT NMs [4]. Fig. S2A is a TEM image of the as-prepared $Cu_{2-x}S$/CNT NMs, revealing that $Cu_{2-x}S$ NPs are decorated on the outer walls of CNTs. The TEM image of $Cu_{2-x}S/C_{dh}$ NMs is provided in Fig. S2B, revealing the size and morphologies of $Cu_{2-x}S$ NPs were different from that in the $Cu_{2-x}S$/C dots. The TEM image of $Cu_{2-x}S$/carbon black NMs displayed in Fig. S2C reveals that the sizes and the morphology of $Cu_{2-x}S$ NPs were different from that in the $Cu_{2-x}S$/C dots and larger aggregates were apparent. The cyclic voltammetry (CV) curves recorded in O_2- and N_2-saturated 0.5 M H_2SO_4 at a scan rate of 50 mV s^{-1} (Fig. S3) revealed that the $Cu_{2-x}S$/C dot NMs were ORR active. The LSV curves of CNT-, C dot-, $Cu_{2-x}S$/carbon black-, $Cu_{2-x}S/C_{dh}$-, $Cu_{2-x}S$/C dot-, $Cu_{2-x}S$/CNT-, and commercial Pt/C-modified RDEs recorded in O_2-saturated 0.5 M H_2SO_4, at a rotation rate of 3600 rpm, and a scan rate of 5 mV s^{-1} are depicted in Fig. 3A. The $Cu_{2-x}S$ mass loading in each electrode was ca. 2.26 mg cm^{-2}. It should be noted that LSV scans were performed from 1.0 to 0 V. The onset potential values for the ORRs using the $Cu_{2-x}S$/CNT and $Cu_{2-x}S$/C dot RDEs are almost identical, ca. 0.92 V vs. Ag/AgCl, which is lower than the onset potential (0.7 V) of the Pt and Pd electrodes [36,37], revealing that $Cu_{2-x}S$/CNT and $Cu_{2-x}S$/C dot RDEs exhibited higher ORR activity. The half-wave potential ($E_{1/2}$) value of a catalyst provides visual insights into its ORR activity. When compared with the commercial Pt/C-modified RDE, the $Cu_{2-x}S$/CNT and $Cu_{2-x}S$/C dot RDEs provided higher $E_{1/2}$ values, revealing their higher ORR activities (Fig. 3A). The limiting current density plateau of both $Cu_{2-x}S$/CNT and $Cu_{2-x}S$/C dot RDEs are well developed over the potential range 0.95 → 0.3 V, revealing more efficient diffusion processes occurred in the former two RDEs [38]. The electron-transfer number (n) was derived from the slopes of Koutecky–Levich plots at various potentials (Fig. 3B), with results of n = 3.5 and 3.8, indicating both two- and four-electron reductions taking place at potentials 0.2 and 0.4 V, respectively. At 0.6 V vs. Ag/AgCl, n was 4, suggesting four-electron reduction of O_2.

The limiting current densities of $Cu_{2-x}S$/CNT and $Cu_{2-x}S$/C dot RDEs for the ORR at 0.6 V were both -1.77 mA cm^{-2} at a rotation rate of 3600 rpm. CNT and C dot RDEs exhibited negligible current density, indicating that the ORR activity was mainly from $Cu_{2-x}S$ NPs. The limiting current density plateau of $Cu_{2-x}S$/carbon black RDE over the potential range 0.95 → 0.3 V (Fig. 3A) was not well defined, indicating a poor diffusion [38]. Moreover, the limiting current density of the $Cu_{2-x}S$/carbon black RDE was smaller than that of $Cu_{2-x}S$/C dot RDE, mainly because of lack of functional groups on their surfaces that results in weaker interactions between carbon black and $Cu_{2-x}S$ NPs, leading to poor ORR activity. Under the same experimental conditions, the $Cu_{2-x}S/C_{dh}$ RDE relative to the $Cu_{2-x}S$/C dots RDE exhibits a smaller limiting current density and higher onset potential for ORR, revealing its poor ORR activity. The ORR activities of the hybrid materials are dependent on the conductivity, surface area, and surface properties of the carbon materials [39]. Our previous study revealed the existence of carboxylate and hydroxyl groups on the surfaces of C dots that were prepared from coffee through the hydrothermal route [16]. C dots prepared from different carbon sources through various approaches have different surface properties and morphologies, which affect the formation of $Cu_{2-x}S$/C dots and thus their ORR activity. The surface functional groups on C_{dh} were different from that on C dots, which affected the nucleation and anchoring of $Cu_{2-x}S$ NPs on C_{dh} that altered their morphology and decreased their ORR efficiency [22]. Similar results were also reported for the nucleation and anchoring of Co_3O_4 on the surface of functionalized reduced graphene oxide [39]. This result suggested different types of carbon supports (e.g., C_{dh} and carbon black) affected the nucleation and anchoring of $Cu_{2-x}S$ NPs, which altered their morphology and their ORR activity.

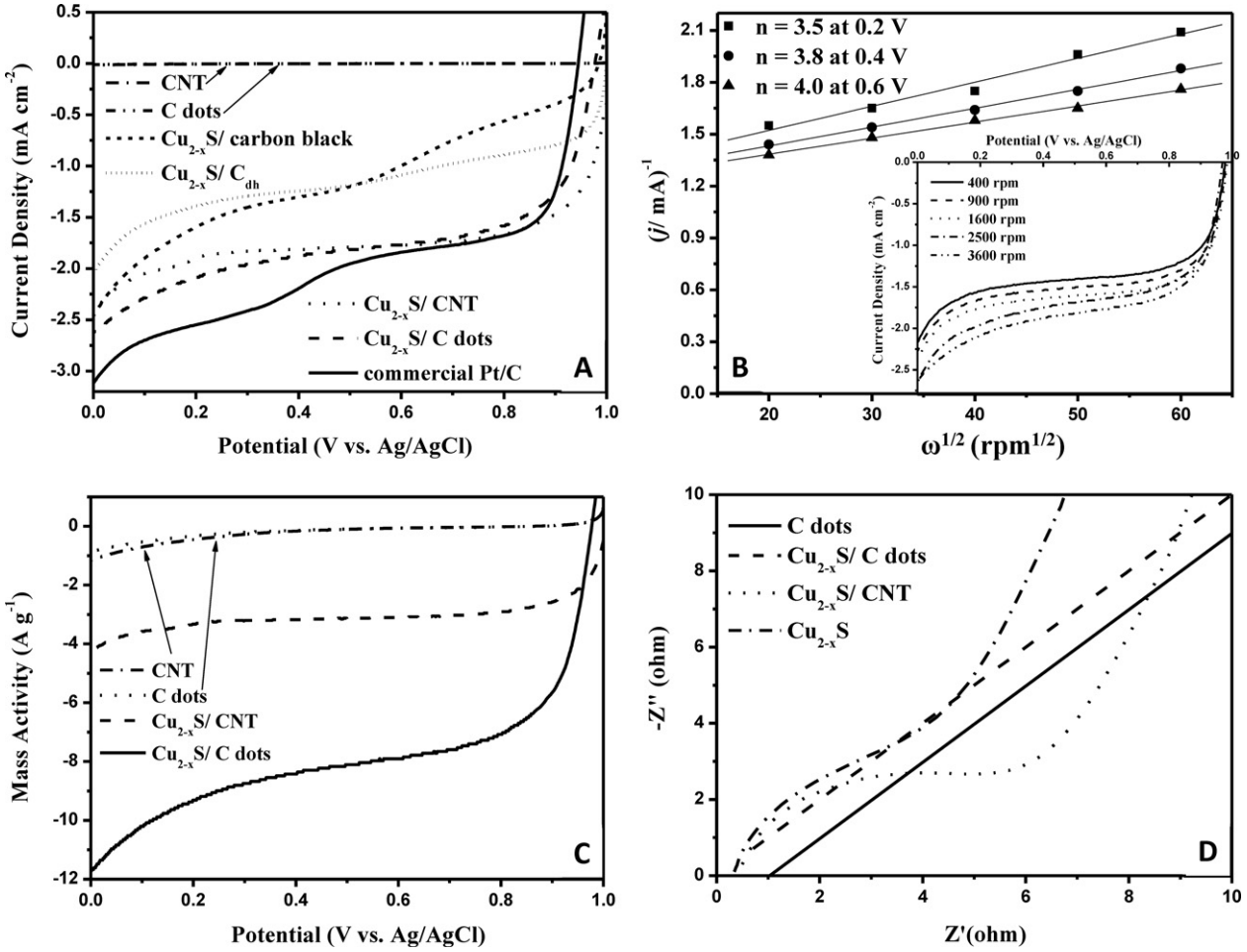

Fig. 3. (A) LSV curves of CNT-, C dots-, $Cu_{2-x}S$/carbon black-, $Cu_{2-x}S/C_{dh}$-, $Cu_{2-x}S$/CNT-, $Cu_{2-x}S$/C dot-, and Pt/C-modified RDEs. (B) Koutecky–Levich plots at different potentials for $Cu_{2-x}S$/C dot RDE curves. Inset: LSV curves of $Cu_{2-x}S$/C dot RDE at different rotation speeds. (C) Mass activities of CNT, C dots, $Cu_{2-x}S$/CNT, and $Cu_{2-x}S$/C dot RDEs in 0.5 M H_2SO_4. (D) Nyquist plots of C dots, $Cu_{2-x}S$/C dots, $Cu_{2-x}S$/CNT, and $Cu_{2-x}S$ RDEs in 0.5 M H_2SO_4. Z' and Z'' are the virtual and real impedances, respectively.

Stable current was not observed at $Cu_{2-x}S$-modified (without C dots) RDE, because it was weakly adhered onto the electrode surface (data not shown). The high ORR catalytic performance of the $Cu_{2-x}S$/CNT and $Cu_{2-x}S$/C dot RDEs is attributed to an intimate coupling between $Cu_{2-x}S$ and supports. The composite nanostructures offer the advantage of a large interfacial area, facilitating the ORR through facile charge transport between oxygen molecules adsorbed on $Cu_{2-x}S$ active sites and the electrode [4]. Though the amounts of CNT in the $Cu_{2-x}S$/CNT RDE were higher than C dots used in the $Cu_{2-x}S$/C dot RDE, still the latter exhibited higher mass activity for the ORR (Fig. 3C). The mass (g) is the sum of $Cu_{2-x}S$ and carbon materials. Growth of $Cu_{2-x}S$ NPs in the presence of C dots furnished smaller-sized $Cu_{2-x}S$ NPs, leading to higher surface area and greater electrocatalytic activity [12,13].

To further understand the interface properties of surface-modified electrodes, we conducted EIS. Fig. S4 illustrates an equivalent circuit model employed to simulate the resulting EIS spectra of the $Cu_{2-x}S$/CNT, $Cu_{2-x}S$/C dot, and $Cu_{2-x}S$ RDEs in Fig. 3D. The R_{ct} value decreased in the order $Cu_{2-x}S > Cu_{2-x}S$/CNT > $Cu_{2-x}S$/C dot RDEs. The $Cu_{2-x}S$/C dot RDE had the lowest R_{ct} value, revealing that the charge transfer was most effective at its interface with the electrolyte. As a result, the highest ORR rate was generated in the $Cu_{2-x}S$/C dot RDE. The $Cu_{2-x}S$/C dot RDE in 0.5 M H_2SO_4 did exhibit slight Warburg diffusion impedance at very low frequencies, suggesting facile charge-transfer dynamics associated with C dots [40]. Inefficient charge transfer occurred at the interface of $Cu_{2-x}S$ NPs and CNT with the electrolyte because $Cu_{2-x}S$ NPs were not well attached to the CNTs as supported by the TEM image shown in Fig. S2A. Density functional theory calculations reveal that the presence of oxygen containing functional groups at the CNTs surface reduced the HOMO–LUMO gap because the 2p electrons of oxygen atoms were overlapped with the π-electron system of CNTs, leading to an easier excitation of electrons from the low-lying occupied levels to the upper empty level that enhanced the chemical reactivity toward the adsorbate [41]. But, such a phenomenon did not occur in the pristine CNTs that were used in our work, mainly because they do not contain any functional groups, resulting in weaker interactions of the CNTs with $Cu_{2-x}S$ NPs and thus poor ORR activity. Thus, we conclude that a synergetic effect between the catalytic activity of $Cu_{2-x}S$ and the sufficient electron transfer provided by the $Cu_{2-x}S$/C dot RDE is responsible for its excellent electrochemical activity toward the ORR.

A good ORR electrocatalyst must be resistant to methanol poisoning. We investigated the Tafel plots (Fig. 4A) by plotting the limiting current density ($\log i$) against the applied voltage (E) in 0.5 M H_2SO_4 with and without 1 M MeOH. The open-circuit potential (OCP) implies the electrical potential of the system that reaches equilibrium without applying any external voltage. OCPs of the $Cu_{2-x}S$/C dot RDE obtained in the absence and presence of 1 M MeOH were 0.50 and 0.51 V (vs. Ag/AgCl), respectively. The slight difference in the OCPs reveals that the as-prepared $Cu_{2-x}S$/C dot electrode exhibited good methanol tolerance. The OCPs of the Pt/C RDE obtained in the absence and presence of 1 M MeOH were 0.69 and 0.48 V (vs. Ag/AgCl), respectively, demonstrating a serious

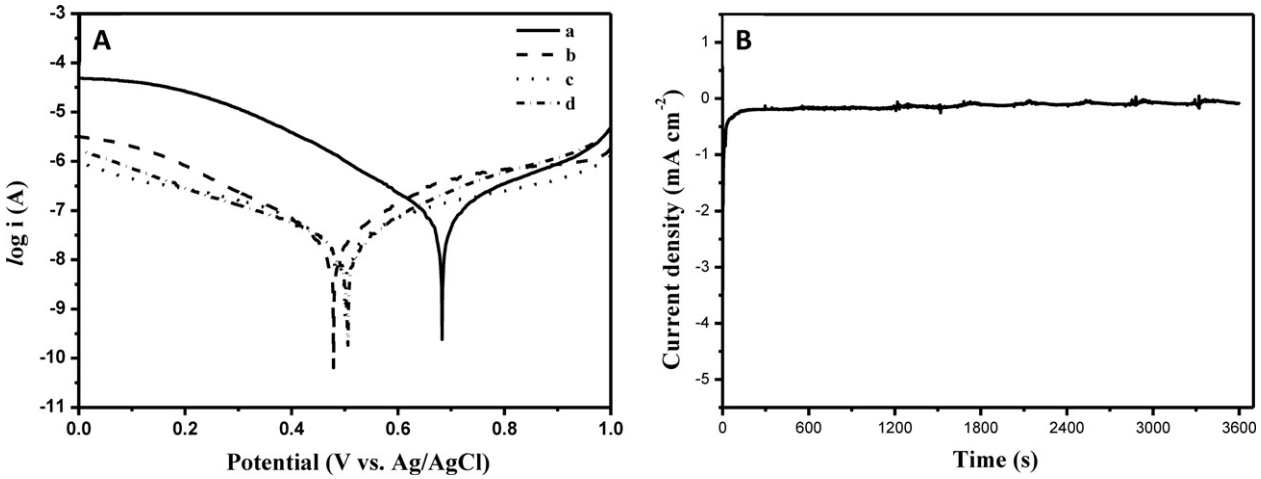

Fig. 4. (A) Tafel plots of (a and b) commercial Pt/C and (c and d) $Cu_{2-x}S$/C dot RDEs. Electrolyte: (a and c) 0.5 M H_2SO_4; (b and d) 0.5 M H_2SO_4 and 1 M MeOH. (B) Chronoamperometric curve of $Cu_{2-x}S$/C dot RDE in 0.5 M H_2SO_4.

MeOH poisoning effect as a result of concomitant depolarization on the Pt/C electrode surface [42,43]. We noted that the OCP value (0.69 V) of the Pt/C RDE relative to the $Cu_{2-x}S$/C dot RDE (0.50 V) was more positive, mainly due to the strong adsorption of hydroxyl groups [44,45]. Fig. 4B displays a chronoamperometry measurement for the $Cu_{2-x}S$/C dot RDE in 0.5 M H_2SO_4, with almost no decay (less than 1% of decay) in the current during the first 3600 s, suggesting that no notable dissolution of $Cu_{2-x}S$ NMs occurred under the hydrodynamic measurement conditions. Besides, the atomic ratio of Cu and S of the $Cu_{2-x}S$/C dot NMs after conducting chronoamperometry did not change in Fig. S5.

4. Conclusions

We found that the C dots assisted in the formation of small-sized $Cu_{2-x}S$ NPs that are bound to the C dots through PVP. The high electrocatalytic activity of $Cu_{2-x}S$/C dot electrodes results mainly from the high activity of $Cu_{2-x}S$ and the efficient electron transfer in the electrode. Having the advantages of facile preparation, low cost, high catalytic activity, and excellent MeOH tolerance, the $Cu_{2-x}S$/C dots show great potential for use as cathodes in DMFCs.

Acknowledgment

This study was financially supported by the National Science Council of Taiwan under contracts NSC 98-2113-M-002-011-MY3 and NSC 100-2627-M-002-007.

Appendix A. Supplementary data

Supplementary data associated with this article can be found, in the online version, at http://dx.doi.org/10.1016/j.apcatb.2012.12.004.

References

[1] A.A. Gewirth, M.S. Thorum, Inorganic Chemistry 49 (2010) 3557–3566.
[2] W. Xiong, F. Du, Y. Liu, A. Perez, M. Supp, T.S. Ramakrishnan, L. Dai, L. Jiang, Journal of the American Chemical Society 132 (2010) 15839–15841.
[3] S. Shanmugam, T. Osaka, Chemical Communications 47 (2011) 4463–4465.
[4] A. Morozan, B. Jousselme, S. Palacin, Energy Environment Science 4 (2011) 1238–1254.
[5] T. Fujigaya, T. Uchinoumi, K. Kaneko, N. Nakashima, Chemical Communications 47 (2011) 6843–6845.
[6] Y. Tang, B.L. Allen, D.R. Kauffman, A. Star, Journal of the American Chemical Society 131 (2009) 13200–13201.
[7] Y. Wang, Q. Li, M. Nie, X. Li, Y. Li, X. Zhong, Nanotechnology 22 (2011) 305401.
[8] Y. Feng, T. He, N. Alonso-Vante, Electrochimica Acta 54 (2009) 5252–5256.
[9] Y. Feng, T. He, N. Alonso-Vante, Chemistry of Materials 20 (2008) 26–28.
[10] B.C.H. Steele, A. Heinzel, Nature 414 (2001) 345–352.
[11] S. Bas, Recent Trends in Fuel Cell Science and Technology, Anamaya, New Delhi, India, 2007.
[12] H. Wang, Y. Liang, Y. Li, H. Dai, Angewandte Chemie International Edition 50 (2011) 10969–10972.
[13] C.-H. Lai, K.-W. Huang, J.-H. Cheng, C.-Y. Lee, B.-J. Hwang, L.-J. Chen, Journal of Materials Chemistry 20 (2010) 6638–6645.
[14] E. Antolini, Applied Catalysis B: Environmental 74 (2007) 324–336.
[15] Y. Xin, J.-g. Liu, Y. Zhou, W. Liu, J. Gao, Y. Xie, Y. Yin, Z. Zou, Journal of Power Sources 196 (2011) 1012–1018.
[16] P.-C. Hsu, Z.-Y. Shih, C.-H. Lee, H.-T. Chang, Green Chemistry 14 (2012) 917–920.
[17] S.-W. Hsu, W. Bryks, A.R. Tao, Chemistry of Materials 24 (2012) 3765–3771.
[18] W. Li, A. Shavel, R. Guzman, J. Rubio-Garcia, C. Flox, J. Fan, D. Cadavid, M. Ibanez, J. Arbiol, J.R. Morante, A. Cabot, Chemical Communications 47 (2011) 10332–10334.
[19] W. Han, L. Yi, N. Zhao, A. Tang, M. Gao, Z. Tang, Journal of the American Chemical Society 130 (2008) 13152–13161.
[20] A.A. Sagade, R. Sharma, I. Sulaniya, Journal of Applied Physics 105 (2009) 043701.
[21] Z. Yang, C.-Y. Chen, H.-T. Chang, Journal of Power Sources 196 (2011) 7874–7877.
[22] S.-L. Hu, K.-Y. Niu, J. Sun, J. Yang, N.-Q. Zhao, X.-W. Du, Journal of Materials Chemistry 19 (2009) 484–488.
[23] P. Hernández-Fernández, S. Rojas, P. Ocón, J.L. Gómez de la Fuente, J. San Fabián, J. Sanza, M.A. Peña, F.J. García-García, P. Terreros, J.L.G. Fierro, Journal of Physical Chemistry C 111 (2007) 2913–2923.
[24] S.N. Baker, G.A. Baker, Angewandte Chemie International Edition 49 (2010) 6726–6744.
[25] H.S. Kim, T.K. Sung, S.Y. Jang, Y. Myung, Y.J. Cho, C.-W. Lee, J. Park, J.-P. Ahn, J.-G. Kim, Y.-j. Kim, CrystEngComm 13 (2011) 2091–2095.
[26] P. Roy, K. Mondal, S.K. Srivastava, Crystal Growth and Design 8 (2008) 1530–1534.
[27] L. Tian, D. Ghosh, W. Chen, S. Pradhan, X. Chang, S. Chen, Chemistry of Materials 21 (2009) 2803–2809.
[28] S.V. Bagul, S.D. Chavhan, R. Sharma, Journal of Physics and Chemistry of Solids 68 (2007) 1623–1629.
[29] W. Lou, M. Chen, X. Wang, W. Liu, Journal of Physical Chemistry C 111 (2007) 9658–9663.
[30] Y. Han, Y. Wang, W. Gao, Y. Wang, L. Jiao, H. Yuan, S. Liu, Powder Technology 212 (2011) 64–68.
[31] L. Andronic, L. Isac, A. Duta, Journal of Photochemistry and Photobiology A 221 (2011) 30–37.
[32] P. Kumar, R. Nagarajan, Inorganic Chemistry 50 (2011) 9204–9206.
[33] J. Shan, P. Pulkkinen, U. Vainio, J. Maijala, J. Merta, H. Jiang, R. Serimaa, E. Kauppinen, H. Tenhu, Journal of Materials Chemistry 18 (2008) 3200–3208.
[34] A. Ghahremaninezhad, E. Asselin, D.G. Dixon, Journal of Physical Chemistry C 115 (2011) 9320–9334.
[35] H. Lee, S.W. Yoon, E.J. Kim, J. Park, Nano Letters 7 (2007) 778–784.
[36] V. Mazumder, M. Chi, K.L. More, S. Sun, Journal of the American Chemical Society 132 (2010) 7848–7849.
[37] M. Shao, K. Shoemaker, A. Peles, K. Kaneko, L. Protsailo, Journal of the American Chemical Society 132 (2010) 9253–9255.
[38] Y. Garsany, O.A. Baturina, K.E. Swider-Lyons, S.S. Kocha, Analytical Chemistry 82 (2010) 6321–6328.
[39] Y. Liang, Y. Li, H. Wang, J. Zhou, J. Wang, T. Regier, H. Dai, Nature Materials 10 (2011) 780–786.

[40] J.G. Radich, R. Dwyer, P.V. Kamat, Journal of Physical Chemistry Letters 2 (2011) 2453–2460.
[41] T. Prasomsri, D. Shi, D.E. Resasco, Chemical Physics Letters 497 (2010) 103–107.
[42] S.D. Lin, T.C. Hsiao, J.R. Chang, A.S. Lin, Journal of Physical Chemistry B 103 (1999) 97–103.
[43] M. Umeda, H. Sugii, I. Uchida, Journal of Power Sources 179 (2008) 489–496.
[44] S.L. Gojković, T.R. Vidaković, D.R. Đurović, Electrochimica Acta 48 (2003) 3607–3614.
[45] E.H. Yu, K. Scott, R.W. Reeve, Journal of Electroanalytical Chemistry 547 (2003) 17–24.